Effect of Electron-phonon Scattering on the Thermal Conductivity of Si Nanowires

Kantawong Vuttivorakulchai, Mathieu Luisier, and Andreas Schenk
Integrated Systems Laboratory, ETH Zurich, CH-8092 Zurich, Switzerland.
Email: kvuttivo@iis.ee.ethz.ch

***Abstract*—Even though the effect of electron-phonon scattering on the electronic properties of Si nanowires has been widely studied, its impact on phonon transport has received much less attention. Recent experiments gave the first evidence of a doping-induced reduction of the thermal conductivity in highly B-doped (~5×10^{19} cm^{-3}) Si nanowires with a diameter of 31 nm. Here, we present a model that can fully explain these data. We also simulated the thermal conductivity of P-doped Si nanowires and found a smaller reduction compared to the B-doped samples. Our model includes the effect of incomplete ionization due to interface states, trapped charges, and the dielectric mismatch between nanowire and its surrounding. This effect is most pronounced close to a doping level of 10^{18} cm^{-3} for B- and P-doped Si nanowires with an electronic diameter of 31 nm at room temperature. In mitigating the dielectric mismatch, both an increasing diameter and coating the nanowire by an oxide reduce the effect of incomplete ionization. At high doping concentration (~5×10^{19} cm^{-3}) it can be neglected.**

I. Introduction

It is well-known that B and P dopants in bulk Si reduce its thermal conductivity in the low-temperature range [1, 2]. Therefore, the doping concentration could be another parameter to improve the figure of merit (ZT) of nanostructures when used as thermoelectric converters. Recent simulations [3] of the thermal conductivity of B-doped Si nanowires with a diameter of 31 nm did not match the experimental data because the effect of electron-phonon scattering was not taken into account. In this paper, electron-phonon scattering is included for the first time to calculate the thermal conductivity of B- and P-doped Si nanowires. The good agreement with the available experimental data validates the theoretical model.

II. Theory and Simulation Approach

The thermal conductivity is modeled in the same way as in our previous work [3, 4], except that the phonon band structure is calculated from first principles here. Therefore, there is no need to parameterize the potentials used in the valence-force-field (VFF) approach. The calculated bulk phonon band structure also fits well to the experimental data of bulk Si. This phonon band structure is used as input to compute the thermal conductivity, where the inverse phonon lifetimes from different scattering processes are added up according to Matthiessen's rule. The expressions of the phonon lifetimes for each scattering mechanism, e.g. isotope mass variation scattering, crystalline boundary scattering, and anharmonicity can be found in Ref. [4]. The parameters (*lF, B, C*) of the boundary and anharmonicity terms are obtained by fitting the thermal conductivity of undoped bulk Si to the experiments. *B* and *C* parameters are kept fixed throughout the subsequent calculations. It is found that $B = 6.83 \times 10^{-20}$ s/K, $C = 149$ K, and $lF = 6.98 \times 10^{-3}$ m, which are close to the parameters used in the VFF method in Ref. [4].

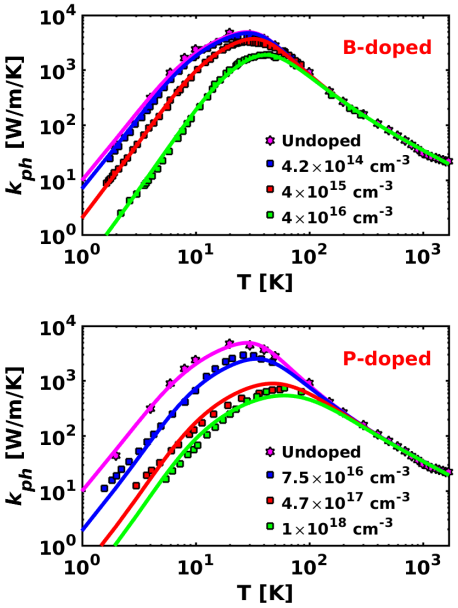

Fig. 1. Bulk thermal conductivity of p-type B-doped Si and n-type P-doped Si. The experimental data have been taken from Refs. [1], [2], [5], and [6].

When Si is doped by B or P, the scattering processes listed above are not sufficient to reproduce the measured thermal conductivity. Two additional mechanisms have to be considered: the mass-difference scattering due to dopants and the scattering due to the lattice distortion caused by dopants [3]. We include these two scattering processes as well as isotope-mass-variation scattering. The missing effect of electron-phonon scattering in Ref. [3] rendered a good fit to the experimental data impossible. When electron-phonon scattering is included, the thermal conductivity can be well reproduced as shown in Fig. 1 for the bulk case.

The thermal conductivity of doped Si nanowires cannot be generally predicted without the effect of incomplete ionization on the free carrier density [7]. For example, the dielectric

mismatch between a nanowire and its surrounding changes the ionization energy of the dopants and, therefore, the number of free charge carriers in the system. Moreover, as the surface-per-volume ratio increases with decreasing diameter, the effect of surface roughness on the thermal conductivity cannot be ignored. A root mean square height $\Delta \approx 0.4$ nm and an auto-correlation length $L = 6$ nm [4] are used here.

A. Phonon band structure of Si from first-principles

First-principles calculations based on projector augmented-wave (PAW) pseudopotentials and the generalized gradient approximation (GGA) with Perdew-Burke-Ernzerhof exchange-correlation functional (PBE) as implemented in the Vienna *ab initio* simulation package (VASP) were performed [8, 9]. A 2×2×2 Monkhorst-Pack $\boldsymbol{k}$-point grid according to 2 $\boldsymbol{k}$-points in the irreducible wedge of the Brillouin zone (BZ) was used. The partial occupancies for each wave function were set by the Gaussian smearing method with 50 meV smearing width of an energy cutoff of 400 eV. For the electronic self-consistency loop, the convergence criteria of 10^{-8} eV/Å force acting on each ion and a total energy difference of 10^{-8} eV between two subsequent iterations were employed to assure highly converged forces. In our simulation, the twelve-atom cubic cell of Si was orientated in ⟨111⟩-direction. A supercell of 360 atoms (2×3×5 conventional cells) was used to evaluate the harmonic interatomic force-constants (IFCs) (Hessian) matrix via density functional perturbation theory. Phonon bands were computed by employing this Hessian matrix.

B. Electron-phonon scattering rates from Golden Rule

Following the derivation in Ref. [10], the transition rate of a phonon with polarization p, frequency ω, and wave vector $\boldsymbol{q}$ caused by electron-phonon scattering can be derived by Fermi's Golden Rule (FGR). Taking into account the dispersion relation of electrons and phonons and performing the integrations, one obtains in the case of a nondegenerate semiconductor [10]

$$\frac{1}{\tau^{\boldsymbol{q},p}_{e/h-ph,1}} = \begin{cases} 2n_f\omega_{\boldsymbol{q},p}\dfrac{(\pi m_{eff})^{1/2}D_A^2}{(2k_B\mathrm{T})^{3/2}\rho_m v_s}\exp\left(-\dfrac{m_{eff}v_s^2}{2k_B\mathrm{T}}\right) & AC \\ n_f(\hbar q)^{-1}\dfrac{(\pi m_{eff})^{1/2}D_o^2}{(2k_B\mathrm{T})^{1/2}\rho_m\omega_o}\sinh\left(\dfrac{\hbar\omega_o}{2k_B\mathrm{T}}\right)\exp\left(-\dfrac{m_{eff}\omega_o^2}{2k_B\mathrm{T}q^2}\right) & OP \end{cases}, \quad (1)$$

where m_{eff} is the density-of-state (DOS) effective mass, ρ_m the mass density, v_s the sound velocity, n_f the carrier (n or p) concentration, ω_o the optical phonon frequency, and T the temperature. D_A (0.23 eV for B-doped Si and 0.06 eV for P-doped Si) and D_o (5×10^7 eV/cm for both cases) are the deformation potential constants for acoustic phonons (AC) and optical phonons (OP), respectively. Our values differ from those in Ref. [10] because the number of equivalent valleys and spin degeneracy used in Ref. [10] are absorbed in our deformation potentials. Other scattering processes are needed to match the experimental data, as shown in the following.

C. Electron-phonon scattering from bound electrons/holes

Interactions between phonons and bound holes/electrons are theoretically described in Refs. [2] and [11]. In Ref. [11] the effect of uniaxial stress on the thermal conductivity of p-type B-doped Si was calculated, when the phonons are scattered by isolated acceptors. The inverse relaxation time of elastic scattering by acceptor holes in the strained crystal is given by

$$\frac{1}{\tau^{\boldsymbol{q},p}_{h-ph,2}} = \frac{\left(2/3\cdot\omega_{\boldsymbol{q},p}D_{h,el}\right)^4 w_p}{100\pi\rho^2 v_s^2\left(S_h^2-\hbar^2\omega_{\boldsymbol{q},p}^2\right)^2}N_{bound,h}f^2\left(\frac{\omega_{\boldsymbol{q},p}}{v_s}\right) \times\left[v_l^{-5}f^2\left(\frac{\omega_{\boldsymbol{q},p}}{v_l}\right)+\frac{3}{2}v_t^{-5}f^2\left(\frac{\omega_{\boldsymbol{q},p}}{v_t}\right)\right], \quad (2)$$

where $D_{h,el}$ is the elastic deformation potential for acceptor holes, v_l (v_t) the longitudinal (transverse) phonon velocity, S_h the energy difference between two doublets caused by applied uniaxial stress or a magnetic field (the external stress is absent here.), $f(q) = [1 - 0.25(a_B)^2\boldsymbol{q}^2]^{-2}$, and a_B the effective Bohr radius. The expression for w_p can be found in Ref. [11], and $N_{bound,h}$ is the density of bound holes discussed in the next section. The inelastic scattering by holes [11] is also considered in our model. Both elastic and inelastic deformation potentials are set to 1.5 eV.

The ground state of a shallow P donor in Si is six-fold degenerate reflecting the 6 equivalent conduction band minima in the effective mass approximation. As consequence of the valley-orbit interaction and the central-cell correction, the triplet is split from the singlet by 11.7 meV, and the doublet lies 1.35 meV above the triplet. Hence, the total energy splitting (S_e) is 13.05 meV. The elastic scattering rate in this case can be written as

$$\frac{1}{\tau^{\boldsymbol{q},p}_{e-ph,2}} = \frac{\left(1/3\cdot\omega_{\boldsymbol{q},p}D_{e,el}\right)^4 wS_e^2}{5\pi\rho^2 v_s^2\left(S_e^2-\hbar^2\omega_{\boldsymbol{q},p}^2\right)^2}f^2\left(\frac{\omega_{\boldsymbol{q},p}}{v_s}\right) \times\left[v_l^{-5}f^2\left(\frac{\omega_{\boldsymbol{q},p}}{v_l}\right)+\frac{3}{2}v_t^{-5}f^2\left(\frac{\omega_{\boldsymbol{q},p}}{v_t}\right)\right] \times\left[2(N_0+N_1)+N_1\left(1+S_e^2/\hbar^2\omega_{\boldsymbol{q},p}^2\right)\right], \quad (3)$$

where $D_{e,el} = 4$ eV and $w = 2/3$. N_0 (N_1) is the number of electrons per unit volume in the singlet (doublet) state. Because S_e is large for Si, N_1 is about zero, and N_0 will be equal to $N_{bound,e}$. The rates of inelastic phonon scattering and thermally-assisted phonon absorption hardly contribute to the total rate [2] and are, therefore, neglected.

D. Incomplete ionization

The equations for the degree of ionization in bulk silicon are given by [12]

$$\frac{N_{ion,e}}{N_{dop,e}} = 1-\frac{1/\left[1+\left(N_{dop}/N_b\right)^d\right]}{1+g\exp\left[\left(E_D-E_F\right)/\left(k_B\mathrm{T}\right)\right]}, E_D = E_C - E_{dop,b}$$
$$\frac{N_{ion,h}}{N_{dop,h}} = 1-\frac{1/\left[1+\left(N_{dop}/N_b\right)^d\right]}{1+g\exp\left[\left(E_F-E_A\right)/\left(k_B\mathrm{T}\right)\right]}, E_A = E_V + E_{dop,b} \quad (4)$$

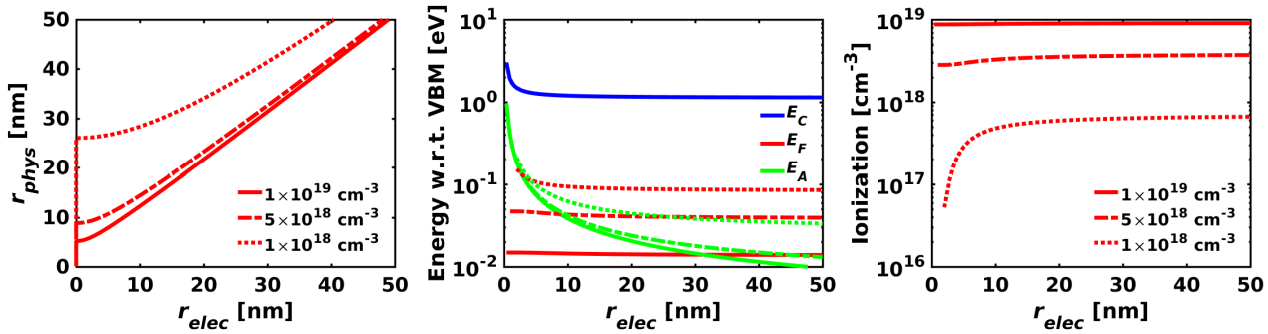

Fig. 2. Physical radius (left), energy level w.r.t. the valence band maximum (VBM) (middle), density of ionized dopants (right) as function of the electronic radius with varying doping concentration of B at room temperature.

where the donor (acceptor) energy level is represented by E_D (E_A) and the ionization energy by $E_{dop,b}$ [12] for bulk. The parameters given in Ref. [12] are used here. With Eq. (4) and the neutrality condition $n + N_{ion,h} = p + N_{ion,e}$ one can calculate N_{bound} which is equal to $N_{dop} - N_{ion}$.

In addition to incomplete ionization in bulk, the free carrier density in Si nanowires is also reduced by the dielectric mismatch between the wire and its surrounding [7]. The occurrence of interface states on the surface of the wire and trapped charges in the native oxide lead to surface depletion of charge carriers [13]. The electronic radius (r_{elec}) is defined as the length in the charge-carrying area from the nanowire center, which differs from the physical radius (r_{phys}),

$$r_{elec} = \sqrt{r_{phys}^2 + \frac{2r_{phys}\left(Q_f - e^2 D_{it}\psi_o\right)}{e\left(N_{dop,e} - N_{dop,h}\right)\left(1 + r_{phys}e^2 D_{it}/\left(2\varepsilon_o\varepsilon_{in}\right)\right)}}. \quad (5)$$

Here, Q_f is the density of fixed oxide charge (assumed to be zero in our case), e the elementary charge, ψ_o the electrostatic potential at $r = 0$, ε_o (ε_{in}) the vacuum (wire) dielectric constant, and D_{it} the interface trapped charge density (6×10^{12} cm^{-2} eV^{-1}). Ref. [14] reported a theoretical study on the band gap energy of nanowires as function of their radius (r_{elec} is used here). This self-energy correction to the tight-binding subband structure that arises from the dielectric mismatch between the nanowires and their environment with dielectric constant (ε_{out}) is given by

$$E_{self} = \frac{e^2}{\varepsilon_o\varepsilon_{in}r_{elec}}\frac{\varepsilon_{in} - \varepsilon_{out}}{\varepsilon_{in} + \varepsilon_{out}}F\left(\frac{\varepsilon_{in}}{\varepsilon_{out}}\right), \quad (6)$$

where the polynomial function F can be found in Ref. [14]. The results of this section including the self-energy correction to the band gap are presented in Figs. 2 and 3. It is assumed that the change in the ionization energy follows $E_{dop} = E_{self} + E_{dop,b}$. This simplistic treatment (similar to Ref. [7]) does not reflect the actual static screening of the Yukawa potential of the randomly distributed dopants in the nanowire dielectric system (with Si, coating oxide, and vacuum).

E. Phonon scattering at surface roughness

Our previous derivation of the surface-roughness scattering rate based on Fermi's Golden Rule [4] is slightly corrected here and reads

$$\frac{1}{\tau_{sr}^{q,p}} = \frac{\omega_{q,p}^2\gamma^2\Delta^2L^2}{8\pi r_{phys}}\sum_{p'}\int_{\omega_{q',p'}=\omega_{q,p}}\frac{dS'}{v_{ph}\left(\omega_{q',p'}\right)}e^{-|q'-q|^2L^2/4}\delta_{q_z'-q_z,0} \quad (7)$$

for a Gaussian auto-correlation function of the roughness. The detailed derivation will be published elsewhere.

III. Results

The calculated thermal conductivities of bulk Si (Fig. 1) and nanowires (Fig. 4) fit well to the available experimental data, which supports our theoretical and simulation approach. The electron-phonon scattering significantly reduces the thermal conductivity in the low-temperature range. This is due to two important mechanisms. The first one (see Eq. (1)) is related to the concentration of all free carriers that are generated by the dopants and interact with the phonon system. However, this interaction alone could not explain the experimentally observed behavior. The second mechanism (see Eqs. (2) and (3)) has its origin in the formation of static strain due to the lattice distortion around the impurity atoms. Both mechanisms are needed to reproduce the measured bulk thermal conductivity.

For nanowires, an additional treatment is required because of the effect of incomplete ionization as experimentally observed in Ref. [7]. Interface states and trapped charges deplete the nanowire near its surface. The charge-carrying area

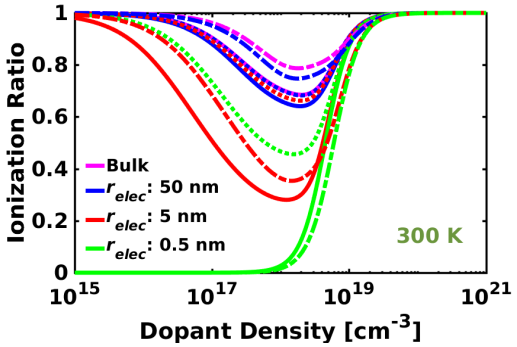

Fig. 3. Ionization ratio as function of doping concentration with different electronic radii at room temperature. Solid lines represent p-type B-doped Si nanowires in air (dielectric constant equals 1.). Dotted lines represent p-type B-doped Si nanowires embedded in Al_2O_3 having a dielectric constant equal to 9. Dash-dotted lines represent n-type P-doped Si nanowires in air.

is reduced as illustrated in Fig. 2 in terms of r_{elec}. It is even possible that the nanowire becomes fully depleted when the radius is small enough or the dopant concentration is low. The dielectric mismatch results in an increase of the ionization energy as function of r_{elec}, i.e. the smaller r_{elec}, the larger E_{dop}.

The ionization ratio in Fig. 3 shows a similar behavior as in Ref. [12] for the bulk case at room temperature. For nanowires, this ratio reduces with decreasing wire radius as expected. It can also be seen that P-doped Si has a higher ionization ratio than B-doped Si in the low-concentration range. A significant improvement of ionization can be achieved when the nanowire is embedded in Al_2O_3, which reduces the dielectric mismatch between Si wire and surrounding. A nanowire with an electronic diameter of 31 nm shows the worst ionization efficiency at a doping concentration of about 10^{18} cm^{-3} (close to the Mott density of bulk Si). Finally, the computed thermal conductivity is shown in Fig. 4. A correction in the low-temperature range is obvious when electron/hole-phonon scattering is included with and without (w/o) surface roughness (SR). Furthermore, n-type P-doped Si nanowires have a higher thermal conductivity than p-type B-doped Si nanowires.

IV. Conclusion

Electron-phonon scattering was included in the calculation of the thermal conductivity of Si nanowires, which improves the match to available experimental data. Incomplete ionization can significantly impact the free carrier concentration around the Mott density. The effect has been treated with a model derived for bulk, but a self-energy correction as function of the electronic radius was added. The actual change of the ionization energy due to the reduced static screening in the nanowire dielectric would require a numerical calculation of the screened Coulomb potential based on the given geometry and materials. As the importance of electron-phonon scattering on the thermal conductivity increases with the doping concentration, in the relevant cases r_{elec} is about the same as r_{phys}, and interface states, trapped charges, and the dielectric mismatch do not alter the ionization energy significantly.

Acknowledgment

We acknowledge funding from the Swiss National Science Foundation through SNF under project 149454 (TORNAD).

References

[1] M. G. Holland, et al., “The effect of impurities on the lattice thermal conductivity of silicon,” Proc. Int. Conf. Physics of Semiconductors, pp. 474-481, July 1962.

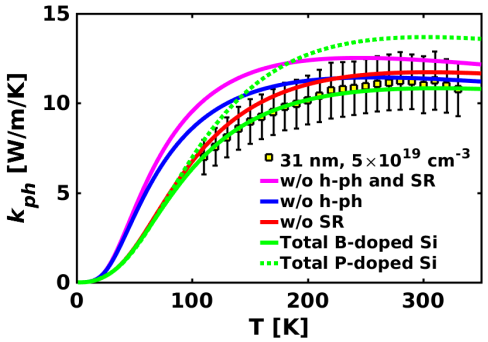

Fig. 4. Thermal conductivity of p-type B-doped Si and n-type P-doped Si nanowires. The experimental data have been taken from Ref. [3].

[2] D. Fortier, et al., “Effect of p donors on thermal phonon scattering in Si,” J. Phys. France, vol. 37, pp. 143-147, February 1976.

[3] S. N. Raja, et al., “Length scale of di□usive phonon transport in suspended thin silicon nanowires,” Nano Lett., vol. 17, pp. 276-283, December 2016.

[4] K. Vuttivorakulchai, et al., “Modeling the thermal conductivity of Si nanowires with surface roughness,” SISPAD, pp. 19-22, September 2016.

[5] C. J. Glassbrenner, et al., “Thermal conductivity of silicon an germanium from 3 K to the melting point,” Phys. Rev., vol. 134, pp. A1058-A1069, May 1964.

[6] M. G. Holland, “Analysis of lattice thermal conductivity,” Phys. Rev., vol. 132, pp. 2461-2471, December 1963.

[7] M. T. Björk, et al., “Donor deactivation in silicon nanostructures,” Nat. Nanotechnol., vol. 3, pp. 103-107, January 2009.

[8] G. Kresse, et al., “Efficient iterative schemes for *ab initio* total-energy calculations using a plane-wave basis set,” Phys. Rev. B, vol. 54, pp. 11169-11186, October 1996.

[9] J. P. Perdew, et al., “Restoring the density-gradient expansion for exchange in solids and surfaces,” Phys. Rev. Lett., vol. 100, pp. 136406, April 2008.

[10] B. Liao, et al., “Significant reduction of lattice thermal conductivity by the electron-phonon interaction in silicon with high carrier concentrations: a first-principles study,” Phys. Rev. Lett., vol. 114, pp. 115901, March 2015.

[11] K. Suzuki, et al., “Effects of uniaxial stress and magnetic field on the low-temperature thermal conductivity of p-type Ge and Si,” J. Phys. Soc. Jpn., vol. 31, pp. 44-53, July 1971.

[12] P. P. Altermatt, et al., “A simulation model for the density of states and for incomplete ionization in crystalline silicon. II. Investigation of Si:As and Si:B and usage in device simulation,” J. Appl. Phys., vol. 100, pp. 113715, August 2006.

[13] V. Schmidt, et al., “Influence of the Si/SiO2 interface on the charge carrier density of Si nanowires,” Appl. Phys. A, vol. 86, pp. 187-191, November 2006.

[14] Y. M. Niquet, et al., “Electronic structure of semiconductor nanowires,” Phys. Rev. B, vol. 73, pp. 165319, April 2006.